

DuetFace: Collaborative Privacy-Preserving Face Recognition via Channel Splitting in the Frequency Domain

Yuxi Mi
yxmi20@fudan.edu.cn
Fudan University
Shanghai, China

Yuge Huang
yugehuang@tencent.com
Tencent Youtu Lab
Shanghai, China

Jiazhen Ji
royji@tencent.com
Tencent Youtu Lab
Shanghai, China

Hongquan Liu
hqliu21@m.fudan.edu.cn
Fudan University
Shanghai, China

Xingkun Xu
xingkunxu@tencent.com
Tencent Youtu Lab
Shanghai, China

Shouhong Ding
ericshding@tencent.com
Tencent Youtu Lab
Shanghai, China

Shuigeng Zhou*
sgzhou@fudan.edu.cn
Fudan University
Shanghai, China

ABSTRACT

With the wide application of face recognition systems, there is rising concern that original face images could be exposed to malicious intents and consequently cause personal privacy breaches. This paper presents DuetFace, a novel privacy-preserving face recognition method that employs collaborative inference in the frequency domain. Starting from a counterintuitive discovery that face recognition can achieve surprisingly good performance with only visually indistinguishable high-frequency channels, this method designs a credible split of frequency channels by their cruciality for visualization and operates the server-side model on non-crucial channels. However, the model degrades in its attention to facial features due to the missing visual information. To compensate, the method introduces a plug-in interactive block to allow attention transfer from the client-side by producing a feature mask. The mask is further refined by deriving and overlaying a facial region of interest (ROI). Extensive experiments on multiple datasets validate the effectiveness of the proposed method in protecting face images from undesired visual inspection, reconstruction, and identification while maintaining high task availability and performance. Results show that the proposed method achieves a comparable recognition accuracy and computation cost to the unprotected ArcFace and outperforms the state-of-the-art privacy-preserving methods. The source code is available at <https://github.com/Tencent/TFace/tree/master/recognition/tasks/duetface>.

*Corresponding author: Shuigeng Zhou, School of Computer Science, and Shanghai Key Lab of Intelligent Information Processing, Fudan University.

Permission to make digital or hard copies of all or part of this work for personal or classroom use is granted without fee provided that copies are not made or distributed for profit or commercial advantage and that copies bear this notice and the full citation on the first page. Copyrights for components of this work owned by others than ACM must be honored. Abstracting with credit is permitted. To copy otherwise, or republish, to post on servers or to redistribute to lists, requires prior specific permission and/or a fee. Request permissions from permissions@acm.org.

MM '22, October 10–14, 2022, Lisbon, Portugal.

© 2022 Association for Computing Machinery.

ACM ISBN 978-1-4503-9203-7/22/10...\$15.00

<https://doi.org/10.1145/3503161.3548303>

CCS CONCEPTS

• **Security and privacy** → **Privacy protections**; • **Computer systems organization** → *Neural networks*.

KEYWORDS

face recognition, data privacy, deep learning, channel splitting

ACM Reference Format:

Yuxi Mi, Yuge Huang, Jiazhen Ji, Hongquan Liu, Xingkun Xu, Shouhong Ding, and Shuigeng Zhou. 2022. DuetFace: Collaborative Privacy-Preserving Face Recognition via Channel Splitting in the Frequency Domain. In *Proceedings of the 30th ACM International Conference on Multimedia (MM '22)*, October 10–14, 2022, Lisbon, Portugal. ACM, New York, NY, USA, 10 pages. <https://doi.org/10.1145/3503161.3548303>

1 INTRODUCTION

Face recognition (FR) has been a phenomenal biometric method for identity authentication, with lots of remarkable breakthroughs gained in recent years. As face recognition is widely incorporated into applications in such as finance, health, and public security, there rises a growing concern about the privacy of sensitive facial images. The *privacy-preserving face recognition* (PPFR) technique thus has arrested the attention of academia and the industry.

In a typical privacy-preserving face recognition scenario, a query face image is collected and held by local devices such as cell phones and webcams. As often constrained by computation power, they outsource the recognition task to a third-party service provider, who infers on a SOTA model pre-trained on massive labeled datasets. For clarity, we thereafter refer to the image holder as the client and the service provider as the server. As the query face here is considered private, the client is not willing to share the raw image with others, including the server.

In the recent decade, vast advancements have been incorporated into PPFR applications. We coarsely categorize them into two branches: the encrypt-based methods build the privacy of the face image on the bricks of cryptographic primitives and security

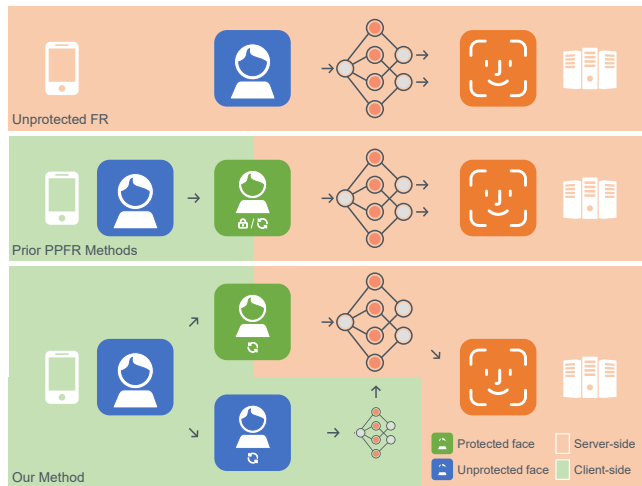


Figure 1: A paradigm comparison among unprotected FR (top), prior PPFR works (middle) and our method (bottom). The images are directly shared in unprotected FR, while are encrypted or transformed in PPFR. The server in prior works performs recognition alone, which usually suffers from a downgrade in accuracy. In our method, the recognition is performed through the collaboration of the server and client.

protocols. Privacy is well protected as long as these bricks are provably or computationally secure. These methods, however, often bear prohibitive computation and communication costs. On the other hand, the transform-based methods perturb or regenerate the face image into a new representation that is visually indistinguishable from the server’s perspective. The drawback of these methods is the almost inevitable participation of noise or loss of information, which results in a downgrade of recognition accuracy. Prior transform-based arts, therefore, generally face a paradoxical trade-off between privacy and accuracy.

Processing images in the frequency domain, first practically employed in the JPEG standard, is a time-honored approach for image compression. As a byproduct, prior researches observe that a small number of low-frequency channels aggregate most of the visual features that are believed crucial for recognition. We advance this observation with a counterintuitive discovery: *the recognition can achieve a surprisingly acceptable accuracy even upon the removal of these crucial channels, while with far less visual information revealed.* We exploit this discovery as a starting point for our work.

Our work employs a transform-based approach as well. Yet, we propose a novel way to effectively solve the privacy-accuracy paradox by addressing them successively through a collaboration between the server and the client. Concretely, let the server possess a SOTA model, whereas the client holds a lightweight model that is an order of magnitude smaller in complexity and cost. We first *split the frequency channels* into two parts by their cruciality for visualization, and let the server infer the non-crucial part. The visual information is therefore concealed from the server and, based on our novel discovery, at the price of tolerable performance degradation. Subsequently, we improve the accuracy by allowing

the client to correct the server-side inaccurate attention on facial features, concretely, by *transferring the client-side attention* to the server through a proposed interactive block. For a better understanding of our idea, a paradigm comparison among unprotected FR, prior PPFR works, and our method is illustrated in Fig. 1. Extensive experiments validate the effectiveness of our scheme.

In summary, the contributions of our paper are three-fold:

- (1) We propose a novel face recognition paradigm by combining the collaborative efforts of two parties: the client and the server. We develop a novel PPFR framework, referred to as DuetFace, which is satisfactory in recognition accuracy, good in cost-efficiency, and reliable in privacy protection;
- (2) We introduce a channel splitting scheme to derive appropriate image break-ups and devise an interactive block based on ROI-refined feature masks to allow attention transfer;
- (3) We conduct extensive experiments on multiple datasets, which validate the effectiveness and superiority of the proposed method.

2 RELATED WORK

2.1 Privacy-Preserving Face Recognition

Significant advances of privacy-preserving face recognition (PPFR) has been achieved significant progress in the past decade, which can be roughly divided into two categories:

Encrypt-based methods. In this branch of work, face recognition is carried out on encrypted domains. Necessary computations such as feature extraction and similarity calculation are either accomplished straightly on the encrypted images or by executing certain security protocols. Pioneering works [9, 15, 27] apply homomorphic encryption (HE) and garbled circuits (GC) to the Eigenface recognition algorithm to hide raw image features from undesired parties. Methods with similar intentions also employ other cryptographic primitives including matrix encryption [17], one-time-pad [8], and functional encryption [1]. Dedicated secure multiparty computation (MPC) schemes are introduced in [19, 38, 41] to perform certain operations (e.g. parameter comparison) in a protected manner, or to outsource parts of the job to a trusted third party.

Encrypt-based methods have very little degradation on the recognition accuracy since almost all the operations involved are lossless. Their effectiveness is also strongly guaranteed by the provable or computational security of the employed cryptographic primitives. However, the practical usages of these methods are limited as they mostly bear intolerable computation costs and communication overhead. Moreover, these methods have low generalizability since most of them are tightly coupled with very specific face recognition schemes. Our work is more generalizable and can achieve competitive accuracy to the standard ArcFace with much less cost.

Transform-based methods. Another active line of research transforms face images into perturbed or regenerated representations to reduce their distinguishability from untrusted parties. For perturbation, differential privacy is employed by lots of works [2, 18, 20, 42] where raw images are overlaid by noise mechanisms to make them less visually differentiable. To increase anonymity, Honda et al. [13] proposed a clustering-based method by mapping raw images to their class representations. As for means to regenerate images into new representations, some works exploit deep-learning-based

methods such as adversarial generative network (GAN) [18, 24] and autoencoder [23], some alter facial landmarks [25], some employ channel shuffling [35], and some remove redundant information by mapping discriminative components into subspaces [3, 16, 22].

These methods usually face a trade-off in balancing privacy and accuracy since the means of protecting the images are performed, in essence, either by bringing in noise or discarding features, which bring in information loss with high probability. Our proposed method overcomes the trade-off and reduces the accuracy loss to a minimum level.

The recently proposed PPF-FD [35] is related to ours as both works study the contribution of channels on visualization and recognition. However, our findings differ from it in two aspects: (1) PPF-FD begins with the premise that the lowest frequency channel contributes not much to the recognition task, which is quite different from ours; (2) The high-frequency channels are removed in PPF-FD as they are believed to contribute little to distinguishability. These channels are instead retained and fully exploited in our work. Further, PPF-FD realizes privacy mainly by randomizing the order of channels, while ours by removing visual components.

2.2 Learning in the Frequency Domain

Learning in the frequency domain is traditionally leveraged for image compression, which allows retaining meaningful patterns for image understanding tasks through compressed representations. Prior arts in face recognition [30, 40] train autoencoder-based networks to perform compression and inference tasks simultaneously. [6] first performs image classification in the frequency domain directly. [39] proposes an accuracy-retaining image down-sampling method, where spatial images are reorganized in the frequency domain to remove the non-crucial channels.

3 METHODOLOGY

3.1 Overview

We here describe the proposed privacy-preserving face recognition method, referred to as DuetFace. In the world of art, a duet is a performance by two singers, instrumentalists, or dancers. Similarly, in DuetFace, the inference is carried out together by two parties, *i.e.*, the server and the client.

Our discovery and motivation. Our work starts from a counter-intuitive discovery. Previous research in the frequency domain [33] suggests that the recognition is mainly determined by channels with lower frequency, which in the meantime are those with larger amplitude [39], as they contribute most of the visual information. Yet, those prior arts mostly ignore the value of the rest “non-crucial” channels. We, on the contrary, surprisingly find that the models can also perform recognition with quite acceptable accuracy by using *only the visually indistinguishable high-frequency channels*. To illustrate this, we train multiple recognition models, each with different numbers of lowest-frequency channels discarded in every color component, then evaluate the trained models on 5 public datasets. Results in Fig. 3(b)(c) show that the models are able to maintain a quite decent performance even the remaining channels possess <10% energy, although there certainly exists an accuracy gap due to the lack of visual information. This discovery allows us to construct our PPF method from a completely different view.

Concretely, we introduce a collaborative paradigm between the server and the client. We first design an appropriate split of the query image in the frequency domain, and let the server train on the high-frequency components in a privacy-preserving manner with tolerable accuracy loss. Then, we let the client further refine the server-side performance by compensating for the missing information without revealing the image itself.

The ability of the server and the client. To better explain the motivation of our method, we start by characterizing the parties. We assume the server to be semi-honest and the client to be resource-sensitive. A semi-honest server is one who honestly follows the face recognition protocol and provides correct results while trying to learn as much as possible from the messages sent by the client. The server is an abstraction of corrupted or unregulated service providers, who may collect, use, and redistribute face images unauthorizedly. A resource-sensitive client is one bounded by limited storage, bandwidth, and computation power. The real-world clients are often reified as personal devices such as cell phones and webcams, whose owners may be unwilling to download and store large models locally or perform complex inference tasks.

The security goals of DuetFace. We address the inference-time privacy between the semi-honest server \mathcal{S} and the client \mathcal{C} . The client possesses a query face image X that it wants the server to identify. The image is considered private. We denote all the information related to X that the client could share without causing a privacy breach as $I(X)$. Our privacy consideration is to prevent the unauthorized collection, use, and redistribution of X , which we concretize into three security goals:

- (1) **Visual privacy.** As the very basis, the server should be unable to collect useful information from the visual appearance of the face image X ;
- (2) **Privacy against reconstruction.** The server may try to reconstruct the information it misses about X . We ergo prescribe, by leveraging $I(X)$, the server cannot effectively produce a reconstruction X' of X ;
- (3) **Privacy against identity inference.** The server could redistribute the reconstructed image to a third party. Plus, the message could be intercepted during transmission. To prevent potential privacy leakage, we require that, without accessing the recognition model, acquiring either $I(X)$ or X' should be insufficient to infer the identity of X .

The paradigm of DuetFace. Let the server and the client each hold a local model M_s and M_c , respectively. Here, M_s is a full-size state-of-the-art model used to answer the recognition requests, whereas M_c is a lightweight model applied as an aid. Both models are pre-trained by the server and M_c is downloaded by the client. To infer a query image X , the client first splits X into two appropriate parts X_s and X_c , where visual information is removed from X_s but retained in X_c . The client shares X_s with the server and keeps X_c to itself. The server identifies X_s via its model M_s . Note that the loss of visual information in X_s will surely degrade the performance of the server-side model. To compensate for the information loss, the client infers the other part X_c of the image X on M_c at a very low computation cost, to obtain a concise supplementary representation $R(X_c)$, which will be revealed to the server. Finally, the server leverages $R(X_c)$ to refine its judgment and produce better results.

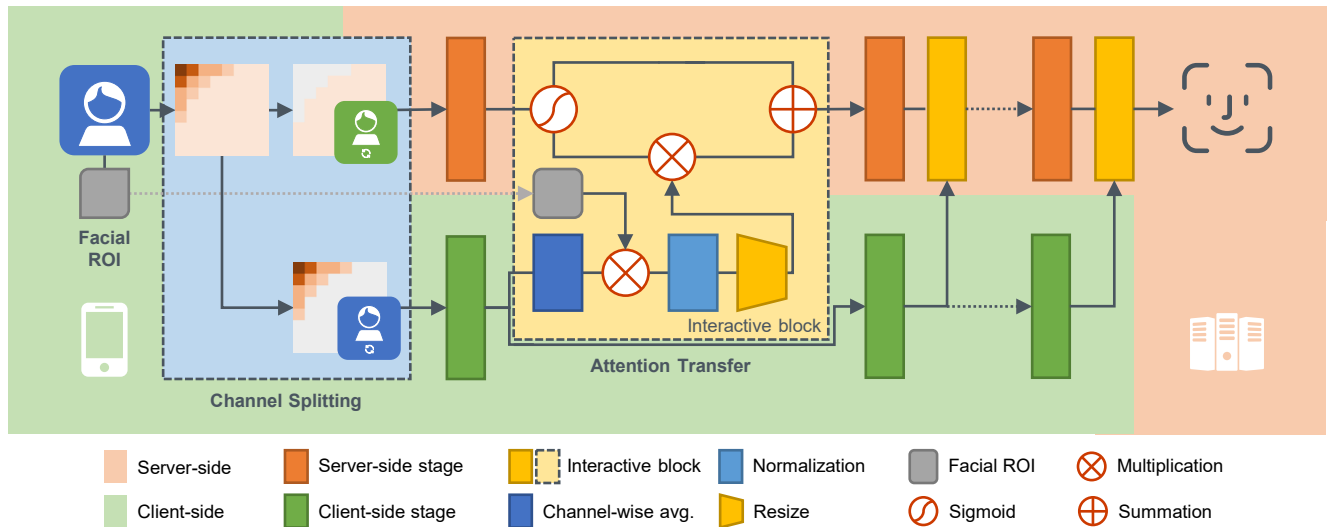


Figure 2: Architecture of DuetFace. The query image is split by the energy of its frequency channels into two parts and inferred separately by the client and the server. To compensate for accuracy loss, an interactive block is plugged in at the end of each stage, where a feature mask transfers the attention from the client to the server. A facial ROI is employed to refine the mask.

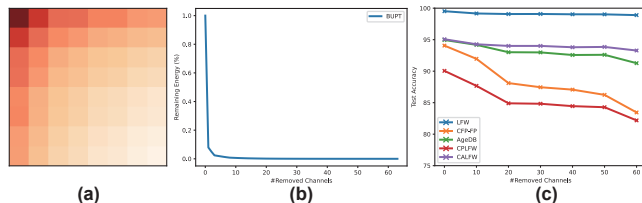


Figure 3: The contributions of channels to visualization and recognition. (a) The low-frequency channels on the top-left account for most of the visual information, in terms of channel energy. (b) The remaining energy sharply decreases as the low-frequency channels are discarded. (c) However, our experiments show that the models are able to maintain decent accuracy even with most visual information removed.

Fig. 2 shows the architecture of DuetFace, which consists of three major components: Channel splitting, attention transfer, and mask denoising. DuetFace is cost-efficient and fulfills the above-mentioned security goals at decent accuracy.

3.2 Splitting Channels in Frequency Domain

As the very first step of our proposed method, the image X is split by channel frequency. To transform the face image to the frequency domain, we first follow the common data pre-processing protocol in the spatial domain to crop, resize and horizontally flip the face image, and obtain an input shape of $H \times W \times 3$. Then, we convert the image from RGB to YCbCr color space and subsequently to the frequency domain by carrying out the block discrete cosine transform (BDCT) following the same way in JPEG compression [32]. We also perform an 8-fold bilinear up-sampling right before BDCT. As standard BDCT maps each 8×8 pixel block into one

frequency channel (here, maps $8H \times 8W \times 3$ to $H \times W \times 192$), the up-sampling enables us to maintain the channel shape and minimize the modifications to the recognition backbone.

We construct a credible split $\{X_s, X_c\}$ of X by the amplitude of channels. Here, we measure amplitude by channel energy: given a channel, its energy is the mean of absolute values of all its elements. We first split channels by energy on the luma (Y) component of YCbCr color space, as it carries most of the visual profiles and features [39]. As shown in Fig. 3(a)(b), the low-frequency channels on the top-left corner contribute to $>90\%$ of total energy. We select K channels with the highest energy as the *crucial channels* and regard the rest as *non-crucial ones*. To achieve spatial consistency, the same selection is also applied to the chroma (Cb, Cr) components. Then, we produce $\{X_s, X_c\}$ utilizing the split channels. We form X_c by concatenating the crucial channels (in the shape of $H \times W \times 3K$), and X_s by the rest. Therefore, visual information is convincingly removed from X_s but retained in X_c , as illustrated in Sec. 4.4.

We adjust the input shapes of the models M_s and M_c to meet the shapes of X_s and X_c , respectively. It is widely observed that discarding non-crucial frequency channels affects the model very slightly [33, 35, 39], so we expect no performance change on M_c . As of M_s , results in Sec. 4.6 show that the model suffers a tolerable accuracy gap in the absence of visual information, which we are to compensate for in the following subsections.

3.3 Attention Transfer

We ascribe the downgrade of M_s to the inaccuracy of model attention. To explain, we visualize the top-down attention maps for each layer of M_s and M_c via Grad-CAM [28]. As shown in Fig. 4, after discarding the crucial channels, the attention of the server-side model M_s could not focus on the effective visual features such as facial contours and the positions of eyes, noses, and lips, which are generally considered the indispensable information for high-quality

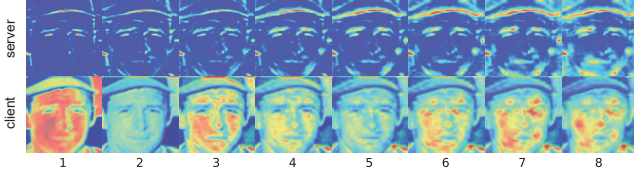


Figure 4: Visualization of each model layer via Grad-CAM. The server-side attention is inaccurate on facial features, while the accurate attention is retained by the client.

face recognition. On the other hand, we observe that accurate attention is retained by the client-side M_c . To restore the missing information in M_s , we propose an *interactive block* IB that teaches the server-side M_s about the attention on the client-side.

Currently, many popular face recognition backbones employ a stage-by-stage architecture to learn features of different levels. Assume M_s and M_c each has n stages, we plug in our interactive block at the end of each stage. Concretely, for face image X , denote the feature maps of M_s, M_c at the end of stage i as $F_i(X_s), F_i(X_c)$, respectively. When querying X , the client first infers X_c on M_c to produce the feature map $F_i(X_c)$, and calculates its channel-wise average to obtain a one-channel feature mask $R_i(X_c)$. The client then normalizes $R_i(X_c)$ to $[0, 1]$ and transmits it to the server. After receiving $R_i(X_c)$, the server first resizes it to align with the height and width of $F_i(X_s)$. Then the server activates its own feature $F_i(X_s)$ by passing it through a sigmoid function and updates it as:

$$F'_i(X_s) = w_i \times (F_i(X_s) \odot R_i(X_c)) + F_i(X_s),$$

where \odot is element-wise multiplication and w_i is a trainable weight that decides the impact of the feature map on the server-side feature.

Note that we use the word “interactive” to describe the function of the block. In practice, the client is not required to jointly compute with the server for each block in real-time. Instead, it just infers M_c once to retrieve and calculate the feature masks of all the stages $R(X_c) = \{R_1(X_c), \dots, R_n(X_c)\}$, and sends it together with X_s to the server. This simplifies the process.

Fig. 5(a) illustrates attention transfer at stages 0 and 1 with samples of the server-side feature map before (left) and after (right) the interactive block, as well as the feature mask $R_i(X_c)$ (middle). The histograms show their corresponding value distributions. As inferred from both visualization and data distribution, the mask effectively transfers knowledge of features such as the entire facial contour (in stage 0) and the approximate positions of eyes and lips (in stage 1) to the server-side. The attention transfer leads to performance improvement of M_s , as demonstrated in Sec. 4.6. To further improve the precision of the feature mask, we also propose a fast and effective denoising method detailed in the following subsection.

3.4 Denoising the Mask by Facial ROI

We subsequently refine the feature mask by removing noisy features. To explain, Fig. 5(b) illustrates some counter-examples that the feature mask can sometimes be ineffective as it incorrectly highlights the hair, the headgear, and the surrounding area, rather than the face itself. Although these features are inherent and could be

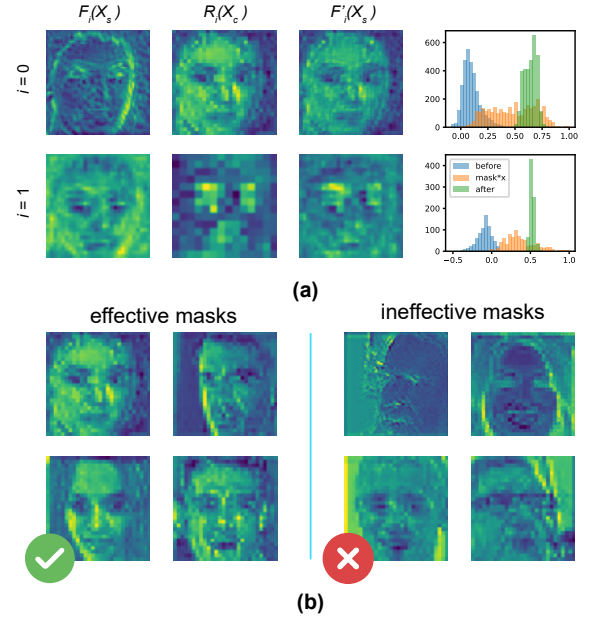


Figure 5: Illustration of attention transfer. (a) The mask $R_i(X_c)$ effectively transfers facial features from the client to the server for correcting the latter’s inaccurate attention. (b) Effective masks highlight the facial contour correctly, while ineffective masks rather highlight the surroundings.

harmless in the standard face recognition process, in our case, they bring in undesirable noise during attention transfer.

We denoise the mask by obtaining a region of interest (ROI) on the raw image. Facial landmark detection is a proven technique that detects and tracks key points in a human face and is widely adopted in applications such as augmented reality. A general facial landmark detector produces a sequence of points that mark the positions of main facial features between facial contours and eyebrows, which specifies the interesting regions of our feature mask. Therefore, we utilize the point sequence to derive the facial ROI.

Specifically, right before performing BDCT, we pass the image X through a pre-trained facial landmark detector to obtain the sequence of landmark points P . Here, we employ an open-source PFLD model [10]. Note that PFLD can be replaced by an arbitrary lightweight 2D landmark detector. Subsequently, we derive the facial ROI, which wraps the facial region, by calculating the convex hull $H(P)$ of P using Delaunay triangulation. Features outside the ROI are considered useless for attention transfer. To remove them, we turn $H(P)$ into a bool mask by marking all the pixels inside as 1 and the rest as 0, and overlay it on its feature masks:

$$R'_i(X_c) = H(P) \odot R_i(X_c).$$

Ergo, a clean mask is produced. Finally, we normalize $R'_i(X_c)$ and use it as a replacement of $R_i(X_c)$.

Fig. 6 show sample masks before and after applying the facial ROI. It can be clearly observed that the ROI removes the features of the surroundings, resulting in focused attention to the face. Results in Sec. 4.6 also show a performance lift after employing the ROI.

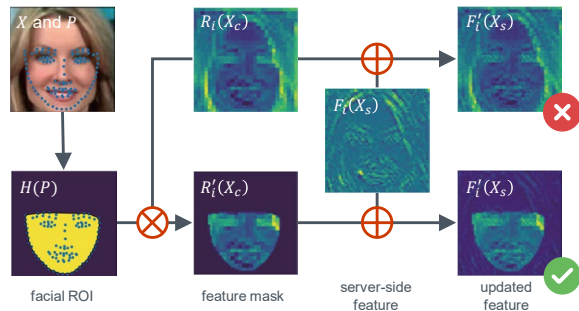


Figure 6: Effect of the facial ROI. After overlaying the ROI, the updated server-side feature shifts its highlight from the noisy surroundings (top) to the correct facial region (bottom).

As a brief summary, the proposed DuetFace successfully overcomes the privacy-accuracy trade-off problem. By performing channel splitting, privacy is guaranteed by removing visual information from the server’s side. Then, the accuracy is compensated by attention transfer from the client-side to the server-side via the ROI-refined feature mask. Sec. 4.3 shows the effectiveness of our method, which almost fills in the accuracy gap with the standard ArcFace, and outperforms those SOTA privacy-preserving counterparts.

4 EXPERIMENTS

4.1 Datasets

Training datasets. We employ MS1Mv2 as training set, plus BUPT-BalancedFace [34] (BUPT in short) for ablation study. MS1Mv2 is refined from MS-Celeb-1M [11] and contains approximately 5.8M images of 85K individuals, whereas BUPT contains 1.8M images from 28K identities. For the training of facial landmark detector, we use Wider Facial Landmarks in-the-wild (WFLW) [37] that contains 10K faces, each with 98 manual annotated landmarks.

Evaluation datasets. We benchmark our method on five popular datasets, including LFW [14], CFP-FP [29], AgeDB [26], CPLFW [43], and CALFW [44]. LFW is the most commonly used evaluation dataset that contains 13K web-collected images from 5.7K identities. CFP-FP, AgeDB, CPLFW and CALFW embody a similar size while focusing on the performance on variations in such as pose and age. We also extend our evaluation to two general, large-scale benchmarks: IJB-B [36] and IJB-C [21].

4.2 Implementation Details

Backbone. We use the adapted ResNet50 with an improved residual unit (IR-50) [12] as the server-side backbone M_s , which has better convergence in the early training stages, and the MobileFaceNet [4] as the client-side M_c . For the client-side facial landmark detection, we apply a PFLD [10] network. Note that both MobileFaceNet and PFLD are lightweight backbones dedicated to resource-constraint devices such as cell phones. We also adapt a smaller IR-18 backbone for ablation study, to explain the generality of our method on different network architectures.

Preparation. We crop and resize each image to 112×112 pixels and add random flipping as image augmentation, then apply BDCT to

obtain 192 frequency components by an open-source TorchJPEG library [7]. After transforming into the frequency domain, we calculate the energy, and select 10 channels from each of the Y, Cb, Cr components as stated in Sec. 3.2. This results in 30 channels selected in total. Note that we choose 30 without loss of generality and it is not the only choice. Therefrom, we form an X_s in the shape of $112 \times 112 \times 162$ and an X_c of $112 \times 112 \times 30$.

We alter the model input channels to meet the shapes of X_c and X_s . Each of the IR-18/50 and MobileFaceNet models contains 4 stages. For attention transfer, we insert an interactive block IB at the end of each stage. Aligning with the feature map shapes in X_s , in our case, the 4 feature masks are resized to the height and width of 56, 28, 14 and 7, respectively. The other parts of the models remain unchanged.

Training. The IR-18/50 and MobileFaceNet models are trained for 24 epochs on the same dataset (either MS1Mv2 or BUPT), using the ArcFace [5] loss. We use the stochastic gradient descent (SGD) optimizer, which is applied with an initial learning rate of 0.1, a momentum of 0.9, and a weight decay of $5e-4$, at a batch size of 512. We successively divide the learning rate by 10 at stages 10, 18, and 22. As of PFLD, we apply a learning rate and a weight decay of $1e-4$ and $1e-6$, respectively, and train it until convergence. Experiments are conducted on 8 NVIDIA Tesla V100 GPU under the PyTorch framework. The same random seed is sampled for all experiments for fairness.

4.3 Comparisons with SOTA Methods

Methods for comparison. We compare DuetFace with two face recognition methods without privacy protection and five state-of-the-art PPFR methods. Specifically: (1) **ArcFace** [5] is the baseline method for RGB images without privacy protection; (2) **ArcFace-FD** is the same ArcFace backbone trained on frequency components instead, which we employ the method in [6]; (3) **PEEP** [2] is the first practical method to introduce differential privacy in PPFR, where we set its privacy budget ϵ to 5; (4) **Cloak** [22] compresses the input feature space by a gradient-based perturbation. We set its accuracy-privacy parameter to 100; (5) **InstaHide** [15] is a lightweight encryption-based method in distributed setting that incorporates the mix-up of k images, which we set to 2; (6) **CPGAN** [31] generates compressive face representations by GAN and local differential privacy; And (7) **PPFR-FD** [35] is a very recent method that masks the face by shuffling and mixing on frequency channels. Results are summarized in Tab. 1.

Results on LFW, CFP-FP, AgeDB, CPLFW, and CALFW are reported by accuracy. Our method achieves a very close performance to the non-privacy-preserving ArcFace baseline. Concretely, our method achieves almost the same performance as ArcFace on LFW, AgeDB and CALFW, and has a limited accuracy drop of 0.51% on CFP-FP, and 0.42% on CPLFW. We believe such accuracy loss is because these two datasets possess more complex variations in pose, which downgrades the inference of facial landmarks. On the other hand, our method takes a leading role over all the SOTA privacy-preserving methods by an advantage from 0.14% to 23.32%. **Results on IJB-B and IJB-C** are reported in TPR@FPR($1e-4$), i.e., the true-positive rate at the false-positive rate of $1e-4$. The TPR of DuetFace is slightly lower than ArcFace, but still outperforms most

Table 1: Comparisons with State-of-the-Art Methods

Method	PPFR	LFW	CFP-FP	AgeDB	CPLFW	CALFW	IJB-B(TPR@FPR)	IJB-C(TPR@FPR)
ArcFace [5]	No	99.77	98.30	97.88	92.77	96.05	94.13	95.60
ArcFace-FD [6]	No	99.78	98.04	98.10	92.48	96.03	94.08	95.64
PEEP [2]	Yes	98.41	74.47	87.47	79.58	90.06	5.82	6.02
Cloak [22]	Yes	98.91	87.97	92.60	83.43	92.18	33.58	33.82
InstaHide [15]	Yes	96.53	83.20	79.58	81.03	86.24	61.88	69.02
CPGAN [31]	Yes	98.87	94.61	96.98	90.43	94.79	92.67	94.31
PPFR-FD [35]	Yes	99.68	95.04	97.37	90.78	95.72	*	94.10
DuetFace (ours)	Yes	99.82	97.79	97.93	92.35	96.10	93.66	95.30

* The results of PPFR-FD are quoted from [34] due to the lack of source code. Please note that its experimental condition may be different slightly from ours.

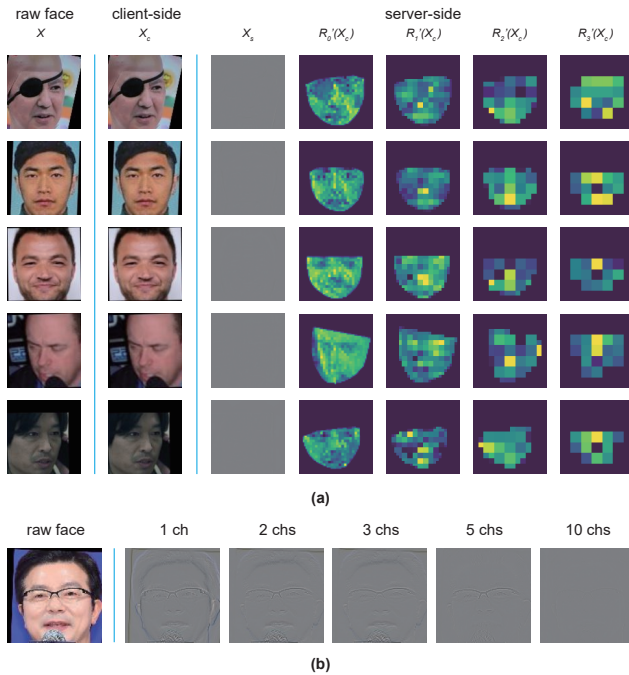


Figure 7: Visual privacy. (a) Illustration of X_s , X_c and $R'_i(X_c)$ on sample images. Perceptible visual information is removed from server-side. (b) We alter the number of crucial channels. As it increases, visual features become indistinguishable.

of its competitors, which indicates our method has good generalizability on large-scale datasets. We also notice that some SOTA methods may fail to generalize well as their performance degrades very sharply.

4.4 Visual Privacy

We validate that our proposed method provides reliable privacy protection that satisfies the security goals stated in Sec. 3.1. The basic concern among our goals is visual security, *i.e.*, the server should not be able to visually inspect the query image by the information it acquires from the client.

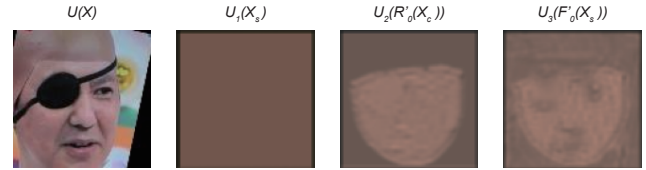


Figure 8: Reconstruction outcomes on X_s , $R'_0(X_c)$ and $F'_0(X_s)$ of sample image via U-Net. The server obtains hardly any visual feature. Reconstruction on the raw face (leftmost) is also provided as a validation of the ability of U-Net.

Visualization of the client/server-side components and feature masks. During the whole inference process, the information the server obtains including the non-crucial components X_s of the query image and the refined feature masks $R'_i(X_c)$ at each stage. To illustrate the effectiveness of our method, we randomly sample face images and visualize their X_s , X_c , and $R'_i(X_c)$. As X_s is in the frequency domain, we pad its removed channels with zero and convert it back to RGB by performing inverse DCT. We perform the same on X_c for comparison. The results in Fig. 7(a) show that most of the perceptible visual information is removed from X_s but retained in X_c , which prevents the server from inspecting X_s while allowing the client to infer X_c (in private) normally. As for the feature masks, the results show that they reveal only very limited visual information such as the approximate facial contours, which would not sabotage our security goal.

Visualization on different numbers of crucial channels. We alter the number of selected channels and visualize their corresponding X_s in Fig. 7(b). Prior work [35] also discards one channel with the highest energy (the direct current component) in its means to protect privacy. Our visualization implies such removal could be insufficient since part of the visual features can still be inferred from the rest components. As the number of selected channels increases, the remaining visual features become indistinguishable.

4.5 Privacy Against Malicious Intent

Ever since its invention, face recognition is under the threat of malicious attacks. Our security goal in Sec. 3.1 addresses concerns to two major forms of inference threats. Specifically, (1) though visually inaccessible, the semi-honest server may still convincingly reconstruct the query image based on what it possesses; And (2)

any third party, if intercepts the information transferred from the client or receives unauthorized redistribution from the server, may infer the identity of the face even without accessing the recognition model. To further demonstrate our method’s ability to protect valuable information about the query face, we impose these two types of threats on DuetFace.

Table 2: Effectiveness Against Reconstruction and Malicious Identity Inference

Target	SSIM↓	PSNR↓	Accuracy↓
Raw image	0.9993	48.30	99.80
X_s	0.5395	13.01	51.52
Reconstruction of X_s	0.5012	12.89	52.03
Reconstruction of $R'_0(X_c)$	0.4422	12.45	57.18
Reconstruction of $F'_0(X_s)$	0.4555	12.63	61.97

Effectiveness against reconstruction. Autoencoders are widely used for reconstruction. In our case, the server may attempt to reconstruct the face image by an autoencoder-based network. Accessible information for the server including the non-crucial channels, the feature masks and their combination, which equals to the masked server-side feature map $F'_i(X_s)$. Ergo, we first infer images randomly picked from MS1Mv2 on a pre-trained DuetFace to collect their X_s , $R'_0(X_c)$ and $F'_0(X_s)$. Note that in our case, as the resolution of feature maps is successively divided by half in each stage, the reconstruction is most likely to succeed on stage 0. We train three autoencoder-based U-Net models, denoted as U_1 , U_2 and U_3 , on X_s , $R'_0(X_c)$ and $F'_0(X_s)$, respectively, then use the trained model for reconstruction. We quantify the quality of the reconstructed images by structural similarity index (SSIM, as compared to the raw image) and peak signal-to-noise ratio (PSNR). As shown in Fig. 8, none of U_1 , U_2 and U_3 manages to effectively reconstruct an image that embodies distinguishable features. And in Tab. 2, we can see that the SSIM and PSNR values are low for all three cases. These verify the robustness of our method against reconstruction.

Effectiveness against identity inference. We subsequently feed X_s (after transformed into the spatial domain) and the reconstructed images into a pre-trained standard ArcFace model and see if they can be recognized. Results are summarized in the last column of Tab. 2. The intention to infer from X_s or its reconstruction $U_1(X_s)$ fails, as the accuracy is slightly higher than random guess (50%). A little accuracy gain is observed on the recognition of $U_2(R'_0(X_c))$ and $U_3(F'_0(X_s))$, as the mask could provide a trace amount of information. Yet, the accuracy remains very low, which thus does not incur an effective threat to our method.

4.6 Ablation Study

We analyze the effects of the major components of DuetFace by testing the performance when removing one of them. Results are reported in Tab. 3 on LFW, CFP-FP, AgeDB, CPLFW, and CALFW. To validate the generality of our method, we also report the results on the combination of the IR-18 model and BUPT dataset.

Effect of the interactive block. The server leverages client-side features to compensate for its inaccurate attention to facial features.

Table 3: Ablation Study Results

Method	LFW	CFP-FP	AgeDB	CPLFW	CALFW
IR-50 + MobileFaceNet, on MS1Mv2					
ArcFace [5]	99.77	98.30	97.88	92.77	96.05
DuetFace	99.82	97.79	97.93	92.35	96.10
w/o IB	99.70	95.86	97.57	90.82	95.86
w/o ROI	99.78	97.23	97.85	92.07	96.06
w/o M_s	99.48	93.91	96.10	89.68	95.08
IR-18 + MobileFaceNet, on BUPT					
ArcFace [5]	99.52	94.06	94.95	90.05	95.07
DuetFace	99.40	93.79	95.07	89.67	95.03
w/o IB	99.16	91.96	94.18	87.67	94.27
w/o ROI	99.39	93.46	95.12	89.03	94.86
w/o M_s	99.32	92.43	93.42	89.15	93.62

* Two sets of experiments are performed in combination of IR-50+MS1Mv2 and IR-18+BUPT to demonstrate the generality of our method.

** ArcFace is the unprotected baseline. “w/o IB ”, “w/o ROI”, “w/o M_s ” correspond to the removal of the interactive block, ROI and server-side model, respectively.

To demonstrate this, we remove the interactive block as well as the client-side model completely and train the server-side M_s alone on X_s . Note that this setting is equal to “w/o M_c ”. From Tab. 3, we observe a <2.5% accuracy degradation.

Effect of facial ROI. The facial ROI refines the feature mask by focusing its attention on the facial region. We remove the facial landmark detector and let the client send the unrefined feature mask directly to the server. We see a notable performance downgrade, especially on CFP-FP and CPLFW. This is possibly because the variety of poses on these two datasets exacerbate attention shifting from the facial region to its surrounding area, which is undesirable.

Performance of the client-side model alone. The client-side model is implemented as an aid to the server-side. A large performance gap is observed between M_c alone and DuetFace, as M_c is much smaller in scale and complexity.

4.7 Complexity and Cost

Table 4: Complexity and Cost of DuetFace

Metric	ArcFace	DuetFace	M_s	M_c
Storage (#param)	43.59M	46.53M	44.03M	2.50M
Time (s/batch)	0.8492	2.2153	1.2165	0.9988
Comm. (#elements)	37,632	35,525	N/A	N/A

To demonstrate the resource-friendliness of our method, we summarize the model size, time cost, and communication overhead required for inference in Tab. 4. As the availability of our method mainly depends on the client-side budget, for a clear demonstration, we list the space and time costs of the client and server separately. The PFLD model is included when evaluating the client’s cost.

Model size. We list the model size by the number of parameters. Since both MobileFaceNet and PFLD are an order of magnitude smaller than the server-side model, the employment of the local

model only accounts for a 6.7% increase of the whole model size and takes about 10M of storage space at the client-side.

Inference time. We perform inference on images with a batch size of 64 and record the average per-batch time. Here, the inference is performed in an asynchronous manner, i.e., the client completes the local computations on all query images, then hands it over to the server for the rest. As compared to ArcFace, our total inference time increased by $\times 2.6$. We think such an increase is marginal as it is the communication time that predominates in real-world practice. The overall time cost is still within a decent scope.

Communication overhead. We calculate by adding up the number of elements in the server-side components X_s and the feature masks of all 4 stages $R'_i(X_c)$. The baseline ArcFace transfers the RGB images of $3 \times 112 \times 112$ directly, resulting in 37,632 elements. In our original purpose, each image is up-sampled before BDCT (as means to preserve the same input height and width), which causes a larger communication cost. We can overcome this by moving the up-sampling later to the server-side. Therefore, the server-side components X_s is of shape $14 \times 14 \times 160$, containing 31,360 elements. On the other hand, the 4 feature masks are the shape of 56×56 , 28×28 , 14×14 , and 7×7 , respectively, which accounts for 4,165 elements in total. Thus, the total element number is 35,525, making our communication overhead similar to that of the baseline ArcFace.

5 CONCLUSION

This paper presents DuetFace, a novel PFR method that achieves high recognition performance through the collaboration between the client and the server. Channel splitting and attention transfer in the frequency domain are leveraged to implement the proposed method. Concretely, our method trains and infers the server-side model on visually indistinguishable non-crucial channels, and compensates for the inaccurate attention by the client-side information, in particular, by producing and transferring a feature mask through a plug-in interactive block. We refine the feature mask by overlaying a facial ROI. Extensive experiments show the proposed method is satisfactory in recognition accuracy, with good cost-efficiency, and achieves high reliability in privacy protection.

REFERENCES

- [1] Michel Abdalla, Florian Bourse, Angelo De Caro, and David Pointcheval. 2015. Simple Functional Encryption Schemes for Inner Products. In *Public-Key Cryptography - PKC 2015 - 18th IACR International Conference on Practice and Theory in Public-Key Cryptography*, Gaithersburg, MD, USA, March 30 - April 1, 2015, *Proceedings (Lecture Notes in Computer Science, Vol. 9020)*, Jonathan Katz (Ed.), Springer, 733–751. https://doi.org/10.1007/978-3-662-46447-2_33
- [2] Mahawaga Arachchige Pathum Chamikara, Peter Bertók, Ibrahim Khalil, Dongxi Liu, and Seyit Camtepe. 2020. Privacy Preserving Face Recognition Utilizing Differential Privacy. *Comput. Secur.* 97 (2020), 101951. <https://doi.org/10.1016/j.cose.2020.101951>
- [3] Thee Chanyaswad, J. Morris Chang, Prateek Mittal, and Sun-Yuan Kung. 2016. Discriminant-component eigenfaces for privacy-preserving face recognition. In *26th IEEE International Workshop on Machine Learning for Signal Processing, MLSP 2016, Vietri sul Mare, Salerno, Italy, September 13-16, 2016*, Francesco A. N. Palmieri, Aurelio Uncini, Kostas I. Diamantaras, and Jan Larsen (Eds.). IEEE, 1–6. <https://doi.org/10.1109/MLSP.2016.7738871>
- [4] Sheng Chen, Yang Liu, Xiang Gao, and Zhen Han. 2018. MobileFaceNets: Efficient CNNs for Accurate Real-Time Face Verification on Mobile Devices. In *Biometric Recognition - 13th Chinese Conference, CCB 2018, Urumqi, China, August 11-12, 2018, Proceedings (Lecture Notes in Computer Science, Vol. 10996)*, Jie Zhou, Yunhong Wang, Zhenan Sun, Zhenhong Jia, Jianjiang Feng, Shiguang Shan, Kurban Ubul, and Zhenhua Guo (Eds.). Springer, 428–438. https://doi.org/10.1007/978-3-319-97909-0_46
- [5] Jiankang Deng, Jia Guo, Niannan Xue, and Stefanos Zafeiriou. 2019. ArcFace: Additive Angular Margin Loss for Deep Face Recognition. In *IEEE Conference on Computer Vision and Pattern Recognition, CVPR 2019, Long Beach, CA, USA, June 16-20, 2019*. Computer Vision Foundation / IEEE, 4690–4699. <https://doi.org/10.1109/CVPR.2019.00482>
- [6] Samuel Felipe dos Santos and Jurandy Almeida. 2021. Less Is More: Accelerating Faster Neural Networks Straight from JPEG. In *Progress in Pattern Recognition, Image Analysis, Computer Vision, and Applications - 25th Iberoamerican Congress, CIARP 2021, Porto, Portugal, May 10-13, 2021, Revised Selected Papers (Lecture Notes in Computer Science, Vol. 12702)*, João Manuel R. S. Tavares, João Paulo Papa, and Manuel González Hidalgo (Eds.). Springer, 237–247. https://doi.org/10.1007/978-3-030-93420-0_23
- [7] Max Ehrlich, Larry Davis, Ser-Nam Lim, and Abhinav Shrivastava. 2020. Quantization Guided JPEG Artifact Correction. In *Computer Vision - ECCV 2020 - 16th European Conference, Glasgow, UK, August 23-28, 2020, Proceedings, Part VIII (Lecture Notes in Computer Science, Vol. 12353)*, Andrea Vedaldi, Horst Bischof, Thomas Brox, and Jan-Michael Frahm (Eds.). Springer, 293–309. https://doi.org/10.1007/978-3-030-58598-3_18
- [8] Ovgu Ozturk Ergun. 2014. Privacy preserving face recognition in encrypted domain. In *2014 IEEE Asia Pacific Conference on Circuits and Systems, APCCAS 2014, Ishigaki, Japan, November 17-20, 2014*. IEEE, 643–646. <https://doi.org/10.1109/APCCAS.2014.7032863>
- [9] Zekeriyä Erkin, Martin Franz, Jorge Guajardo, Stefan Katzenbeisser, Inald Lavendijk, and Tomas Toft. 2009. Privacy-Preserving Face Recognition. In *Privacy Enhancing Technologies, 9th International Symposium, PETS 2009, Seattle, WA, USA, August 5-7, 2009, Proceedings (Lecture Notes in Computer Science, Vol. 5672)*, Ian Goldberg and Mikhail J. Atallah (Eds.). Springer, 235–253. https://doi.org/10.1007/978-3-642-01368-7_14
- [10] Xiaojie Guo, Siyuan Li, Jiawan Zhang, Jiayi Ma, Lin Ma, Wei Liu, and Haibin Ling. 2019. PFLD: A Practical Facial Landmark Detector. (2019). [arXiv:1902.10859](https://arxiv.org/abs/1902.10859)
- [11] Yandong Guo, Lei Zhang, Yuxiao Hu, Xiaodong He, and Jianfeng Gao. 2016. MS-Celeb-1M: A Dataset and Benchmark for Large-Scale Face Recognition. In *Computer Vision - ECCV 2016 - 14th European Conference, Amsterdam, The Netherlands, October 11-14, 2016, Proceedings, Part III (Lecture Notes in Computer Science, Vol. 9907)*, Bastian Leibe, Jiri Matas, Nicu Sebe, and Max Welling (Eds.). Springer, 87–102. https://doi.org/10.1007/978-3-319-46487-9_6
- [12] Kaiming He, Xiangyu Zhang, Shaoqing Ren, and Jian Sun. 2016. Deep Residual Learning for Image Recognition. In *2016 IEEE Conference on Computer Vision and Pattern Recognition, CVPR 2016, Las Vegas, NV, USA, June 27-30, 2016*. IEEE Computer Society, 770–778. <https://doi.org/10.1109/CVPR.2016.90>
- [13] Katsuhiko Honda, Masahiro Omori, Seiki Ubukata, and Akira Notsu. 2015. A study on fuzzy clustering-based k-anonymization for privacy preserving crowd movement analysis with face recognition. In *7th International Conference of Soft Computing and Pattern Recognition, SocPar 2015, Fukuoka, Japan, November 13-15, 2015*, Mario Köppen, Bing Xue, Hideyuki Takagi, Ajith Abraham, Azah Kamilah Muda, and Kun Ma (Eds.). IEEE, 37–41. <https://doi.org/10.1109/SOCPar.2015.7492779>
- [14] Gary B. Huang, Manu Ramesh, Tamara Berg, and Erik Learned-Miller. 2007. *Labeled Faces in the Wild: A Database for Studying Face Recognition in Unconstrained Environments*. Technical Report 07-49. University of Massachusetts, Amherst.
- [15] Yangsibo Huang, Zhao Song, Kai Li, and Sanjeev Arora. 2020. InstaHide: Instance-hiding Schemes for Private Distributed Learning. In *Proceedings of the 37th International Conference on Machine Learning, ICML 2020, 13-18 July 2020, Virtual Event (Proceedings of Machine Learning Research, Vol. 119)*. PMLR, 4507–4518. <http://proceedings.mlr.press/v119/huang20i.html>
- [16] Tom A. M. Kevenaar, Geert Jan Schrijen, Michiel van der Veen, Anton H. M. Akkermans, and Fei Zuo. 2005. Face Recognition with Renewable and Privacy Preserving Binary Templates. In *Proceedings of the Fourth IEEE Workshop on Automatic Identification Advanced Technologies (AutoID 2005), 16-18 October 2005, Buffalo, NY, USA*. IEEE Computer Society, 21–26. <https://doi.org/10.1109/AUTOID.2005.24>
- [17] Xiaoyu Kou, Ziling Zhang, Yuelei Zhang, and Linlin Li. 2021. Efficient and Privacy-preserving Distributed Face Recognition Scheme via FaceNet. In *ACM TURC 2021: ACM Turing Award Celebration Conference - Hefei, China, 30 July 2021 - 1 August 2021*. ACM, 110–115. <https://doi.org/10.1145/3472634.3472661>
- [18] Yuancheng Li, Yimeng Wang, and Daoxing Li. 2019. Privacy-preserving lightweight face recognition. *Neurocomputing* 363 (2019), 212–222. <https://doi.org/10.1016/j.neucom.2019.07.039>
- [19] Zhuo Ma, Yang Liu, Ximeng Liu, Jianfeng Ma, and Kui Ren. 2019. Lightweight Privacy-Preserving Ensemble Classification for Face Recognition. *IEEE Internet Things J.* 6, 3 (2019), 5778–5790. <https://doi.org/10.1109/JIOT.2019.2905555>
- [20] Yunlong Mao, Shanhe Yi, Qun Li, Jinghao Feng, Fengyuan Xu, , and Sheng Zhong. 2018. A Privacy-Preserving Deep Learning Approach for Face Recognition with Edge Computing. (July 2018). <https://www.usenix.org/conference/hotedge18/presentation/mao>
- [21] Brianna Maze, Jocelyn C. Adams, James A. Duncan, Nathan D. Kalka, Tim Miller, Charles Otto, Anil K. Jain, W. Tyler Niggel, Janet Anderson, Jordan Cheney, and Patrick Grother. 2018. IARPA Janus Benchmark - C: Face Dataset and Protocol.

- In *2018 International Conference on Biometrics, ICB 2018, Gold Coast, Australia, February 20-23, 2018*. IEEE, 158–165. <https://doi.org/10.1109/ICB2018.2018.00033>
- [22] Fatemehsadat Mireshghallah, Mohammadkazem Taram, Ali Jalali, Ahmed Taha Elthakeb, Dean M. Tullsen, and Hadi Esmaeilzadeh. 2021. Not All Features Are Equal: Discovering Essential Features for Preserving Prediction Privacy. In *WWW '21: The Web Conference 2021, Virtual Event / Ljubljana, Slovenia, April 19-23, 2021*, Jure Leskovec, Marko Grobelnik, Marc Najork, Jie Tang, and Leila Zia (Eds.). ACM / IW3C2, 669–680. <https://doi.org/10.1145/3442381.3449965>
- [23] Vahid Mirjalili, Sebastian Raschka, Anoop M. Nambodiri, and Arun Ross. 2018. Semi-adversarial Networks: Convolutional Autoencoders for Imparting Privacy to Face Images. In *2018 International Conference on Biometrics, ICB 2018, Gold Coast, Australia, February 20-23, 2018*. IEEE, 82–89. <https://doi.org/10.1109/ICB2018.2018.00023>
- [24] Vahid Mirjalili, Sebastian Raschka, and Arun Ross. 2018. Gender Privacy: An Ensemble of Semi Adversarial Networks for Confounding Arbitrary Gender Classifiers. In *9th IEEE International Conference on Biometrics Theory, Applications and Systems, BTAS 2018, Redondo Beach, CA, USA, October 22-25, 2018*. IEEE, 1–10. <https://doi.org/10.1109/BTAS.2018.8698605>
- [25] Vahid Mirjalili and Arun Ross. 2017. Soft biometric privacy: Retaining biometric utility of face images while perturbing gender. In *2017 IEEE International Joint Conference on Biometrics, IJCB 2017, Denver, CO, USA, October 1-4, 2017*. IEEE, 564–573. <https://doi.org/10.1109/IJCB.2017.8272743>
- [26] Stylianos Moschoglou, Athanasios Papaioannou, Christos Sagonas, Jiankang Deng, Irene Kotsia, and Stefanos Zafeiriou. 2017. AgeDB: The First Manually Collected, In-the-Wild Age Database. In *2017 IEEE Conference on Computer Vision and Pattern Recognition Workshops, CVPR Workshops 2017, Honolulu, HI, USA, July 21-26, 2017*. IEEE Computer Society, 1997–2005. <https://doi.org/10.1109/CVPRW.2017.250>
- [27] Ahmad-Reza Sadeghi, Thomas Schneider, and Immo Wehrenberg. 2009. Efficient Privacy-Preserving Face Recognition. In *Information, Security and Cryptology - ICISC 2009, 12th International Conference, Seoul, Korea, December 2-4, 2009, Revised Selected Papers (Lecture Notes in Computer Science, Vol. 5984)*, Dong Hoon Lee and Seokhie Hong (Eds.). Springer, 229–244. https://doi.org/10.1007/978-3-642-14423-3_16
- [28] Ramprasath R. Selvaraju, Michael Cogswell, Abhishek Das, Ramakrishna Vedantam, Devi Parikh, and Dhruv Batra. 2020. Grad-CAM: Visual Explanations from Deep Networks via Gradient-Based Localization. *Int. J. Comput. Vis.* 128, 2 (2020), 336–359. <https://doi.org/10.1007/s11263-019-01228-7>
- [29] Soumyadip Sengupta, Jun-Cheng Chen, Carlos Domingo Castillo, Vishal M. Patel, Rama Chellappa, and David W. Jacobs. 2016. Frontal to profile face verification in the wild. In *2016 IEEE Winter Conference on Applications of Computer Vision, WACV 2016, Lake Placid, NY, USA, March 7-10, 2016*. IEEE Computer Society, 1–9. <https://doi.org/10.1109/WACV.2016.7477558>
- [30] Robert Torfason, Fabian Mentzer, Eirikur Agustsson, Michael Tschannen, Radu Timofte, and Luc Van Gool. 2018. Towards Image Understanding from Deep Compression Without Decoding. (2018). <https://openreview.net/forum?id=HkXWCMbRW>
- [31] Bo-Wei Tseng and Pei-Yuan Wu. 2020. Compressive Privacy Generative Adversarial Network. *IEEE Trans. Inf. Forensics Secur.* 15 (2020), 2499–2513. <https://doi.org/10.1109/TIFS.2020.2968188>
- [32] Gregory K. Wallace. 1991. The JPEG Still Picture Compression Standard. *Commun. ACM* 34, 4 (1991), 30–44. <https://doi.org/10.1145/103085.103089>
- [33] Haohan Wang, Xindi Wu, Zeyi Huang, and Eric P. Xing. 2020. High-Frequency Component Helps Explain the Generalization of Convolutional Neural Networks. In *2020 IEEE/CVF Conference on Computer Vision and Pattern Recognition, CVPR 2020, Seattle, WA, USA, June 13-19, 2020*. Computer Vision Foundation / IEEE, 8681–8691. <https://doi.org/10.1109/CVPR42600.2020.00871>
- [34] Mei Wang and Weihong Deng. 2019. Mitigate Bias in Face Recognition using Skewness-Aware Reinforcement Learning. (2019). arXiv:1911.10692 <http://arxiv.org/abs/1911.10692>
- [35] Yinggui Wang, Jian Liu, Man Luo, Le Yang, and Li Wang. 2022. Privacy-Preserving Face Recognition in the Frequency Domain. (2022). (in press).
- [36] Cameron Whitelam, Emma Taborsky, Austin Blanton, Brianna Maze, Jocelyn C. Adams, Tim Miller, Nathan D. Kalka, Anil K. Jain, James A. Duncan, Kristen Allen, Jordan Cheney, and Patrick Grother. 2017. IARPA Janus Benchmark-B Face Dataset. In *2017 IEEE Conference on Computer Vision and Pattern Recognition Workshops, CVPR Workshops 2017, Honolulu, HI, USA, July 21-26, 2017*. IEEE Computer Society, 592–600. <https://doi.org/10.1109/CVPRW.2017.87>
- [37] Wayne Wu, Chen Qian, Shuo Yang, Quan Wang, Yici Cai, and Qiang Zhou. 2018. Look at Boundary: A Boundary-Aware Face Alignment Algorithm. In *2018 IEEE Conference on Computer Vision and Pattern Recognition, CVPR 2018, Salt Lake City, UT, USA, June 18-22, 2018*. Computer Vision Foundation / IEEE Computer Society, 2129–2138. <https://doi.org/10.1109/CVPR.2018.00227>
- [38] Can Xiang, Chunming Tang, Yunlu Cai, and Qiuxia Xu. 2016. Privacy-preserving face recognition with outsourced computation. *Soft Comput.* 20, 9 (2016), 3735–3744. <https://doi.org/10.1007/s00500-015-1759-5>
- [39] Kai Xu, Minghai Qin, Fei Sun, Yuhao Wang, Yen-Kuang Chen, and Fengbo Ren. 2020. Learning in the Frequency Domain. In *2020 IEEE/CVF Conference on Computer Vision and Pattern Recognition, CVPR 2020, Seattle, WA, USA, June 13-19, 2020*. Computer Vision Foundation / IEEE, 1737–1746. <https://doi.org/10.1109/CVPR42600.2020.00181>
- [40] Kai Xu, Zhikang Zhang, and Fengbo Ren. 2018. LAPRAN: A Scalable Laplacian Pyramid Reconstructive Adversarial Network for Flexible Compressive Sensing Reconstruction. In *Computer Vision - ECCV 2018 - 15th European Conference, Munich, Germany, September 8-14, 2018, Proceedings, Part X (Lecture Notes in Computer Science, Vol. 11214)*, Vittorio Ferrari, Martial Hebert, Cristian Sminchisescu, and Yair Weiss (Eds.). Springer, 491–507. https://doi.org/10.1007/978-3-030-01249-6_30
- [41] Xiaopeng Yang, Hui Zhu, Rongxing Lu, Ximeng Liu, and Hui Li. 2018. Efficient and Privacy-Preserving Online Face Recognition Over Encrypted Outsourced Data. In *IEEE International Conference on Internet of Things (iThings) and IEEE Green Computing and Communications (GreenCom) and IEEE Cyber, Physical and Social Computing (CPSCom) and IEEE Smart Data (SmartData), iThings/GreenCom/CPSCom/SmartData 2018, Halifax, NS, Canada, July 30 - August 3, 2018*. IEEE, 366–373. https://doi.org/10.1109/Cybermatics_2018.2018.00089
- [42] Chen Zhang, Xiongwei Hu, Yu Xie, Maoguo Gong, and Bin Yu. 2019. A Privacy-Preserving Multi-Task Learning Framework for Face Detection, Landmark Localization, Pose Estimation, and Gender Recognition. *Frontiers Neurobotics* 13 (2019), 112. <https://doi.org/10.3389/fnbot.2019.00112>
- [43] T. Zheng and W. Deng. 2018. *Cross-pose LFW: A database for studying cross-pose face recognition in unconstrained environments*. Technical Report 18-01. Beijing University of Posts and Telecommunications.
- [44] Tianyue Zheng, Weihong Deng, and Jiani Hu. 2017. Cross-Age LFW: A Database for Studying Cross-Age Face Recognition in Unconstrained Environments. (2017). arXiv:1708.08197 <http://arxiv.org/abs/1708.08197>